

MIT Open Access Articles

Ultrafast signatures of spin and orbital order in the antiferromagnetic Mott insulator Sr₂CrO₄

The MIT Faculty has made this article openly available. **Please share** how this access benefits you. Your story matters.

Citation: Lee, Min-Cheol, Occhialini, Connor, Li, Jiariu, Zhu, Zhihai, Mix, LT et al. 2021. "Ultrafast signatures of spin and orbital order in the antiferromagnetic Mott insulator Sr₂CrO₄." Conference on Lasers and Electro-Optics.

As Published: 10.1364/CLEO_QELS.2021.FF2L.2

Publisher: The Optical Society

Persistent URL: <https://hdl.handle.net/1721.1/141451>

Version: Author's final manuscript: final author's manuscript post peer review, without publisher's formatting or copy editing

Terms of use: Creative Commons Attribution-Noncommercial-Share Alike



Ultrafast signatures of spin and orbital order in antiferromagnetic α - Sr_2CrO_4

Min-Cheol Lee,¹ Connor Occhialini,² Jiarui Li,² Zhihai Zhu,^{2,3} Nicholas S. Sirica,¹
L. T. Mix,¹ Dmitry A. Yarotski,¹ Riccardo Comin,² and Rohit P. Prasankumar^{1,*}

¹*Center for Integrated Nanotechnologies, Los Alamos National Laboratory, Los Alamos, NM, USA[†]*

²*Department of Physics, Massachusetts Institute of Technology, Cambridge, MA, USA*

³*Beijing National Laboratory for Condensed Matter Physics,*

Institute of Physics, Chinese Academy of Sciences, Beijing 100190, China

(Dated: October 28, 2021)

We used femtosecond optical spectroscopy to study ultrafast spin and orbital ordering dynamics in the antiferromagnetic Mott insulator α - Sr_2CrO_4 . This chromate system possesses multiple spin and orbital ordered phases, and therefore could enable us to study the unique interplay between these collective phases through their non-equilibrium response to photoexcitation. Here, by varying the pump photon energy, we selectively drove inter-site spin hopping between neighboring Cr t_{2g} orbitals and charge transfer-type transitions between oxygen $2p$ and Cr e_g orbitals. The resulting transient reflectivity dynamics revealed temperature-dependent anomalies across the Néel temperature for spin ordering as well as the transition temperatures linked to different types of orbital order. Our results reveal distinct relaxation timescales for spin and orbital orders in α - Sr_2CrO_4 and provide experimental evidence for the phase transition at T_O , possibly related to antiferro-type orbital ordering.

Transition metal (TM) compounds provide a versatile platform for exploring a wide variety of strongly correlated phenomena, such as high- T_C superconductivity, multiferroicity, or novel magnetism [1–3]. These phenomena are accompanied by various types of charge, spin and orbital orders, arising from competition between interactions such as the local crystal field, inter-site exchange interactions, spin-orbit coupling and on-site Coulomb repulsion [3]. Several phase transitions can occur in a single compound at different temperatures, as observed in multi-orbital systems with partially filled d -shells, including cuprates [4], manganites [5, 6], and ruthenates [7].

Chromates are an intriguing member of this class of materials, due to their active degrees of freedom (DOFs), multiple electronic symmetry breaking pathways, and competing order parameters. The case of α - Sr_2CrO_4 is particularly interesting, as it has been shown to exhibit multiple spin and orbital ordering transitions in the Mott insulating ground state (Fig. 1(a)) [8–12]. α - Sr_2CrO_4 presents a unique electronic configuration, with two electrons in t_{2g} orbitals and total spin of $S = 1$. Recent resonant X-ray scattering (RXS) [8] and neutron powder diffraction studies [9] demonstrated antiferromagnetic (AFM) order by tracking a magnetic Bragg peak below the Néel temperature ($T_N = 112$ K), consistent with the temperature (T)-dependent magnetic susceptibility [10]. The RXS study also revealed another in-plane order below $T_S = 50$ K [8], which was attributed to stripe-type spin-orbital order in the d_{yz}/d_{zx} orbital sub-manifold (Fig. 1(a)). α - Sr_2CrO_4 also manifests a signature of a broad transition around $T_O = 140$ K in the specific heat, which is likely unrelated to spin order, as the magnetic susceptibility follows a typical Curie-Weiss

law across T_O [10]. The exact origin of this feature has not been unveiled yet, though it was suggested to arise from a distinct antiferro(AF)-type orbital order in the d_{yz} and d_{zx} orbitals (Fig. 1(a)), as in Sr_2VO_4 [10, 13]. Therefore, more experimental insight is needed to unravel the origin of this phase transition at T_O above the Néel temperature.

In this context, ultrafast optical spectroscopy (UOS) is a powerful tool for providing new insight into the intertwined spin and orbital DOFs in TM compounds [14]. By using femtosecond (fs) photoexcitation to drive the system out of equilibrium, the interplay among the competing charge, spin and orbital DOFs can be disentangled via their different timescales for returning to the initial ground state, as exemplified in previous studies of various TM oxides [16–20, 22–24]. However, to the best of our knowledge this technique has not yet been used to study α - Sr_2CrO_4 , providing an exciting opportunity to shed new light on the origin of the various order parameters present in this system.

In this work, we thus investigate the non-equilibrium dynamics of spin and orbital order in α - Sr_2CrO_4 by measuring the transient changes in reflectivity at 1.55 eV after femtosecond optical photoexcitation. Importantly, by varying the pump photon energy, we can selectively drive specific microscopic processes that trigger clear T -dependent anomalies across the spin and orbital order temperatures. Photoexcitation at 1.0 eV directly perturbs spin and orbital order by inducing spin hopping between neighboring Cr⁴⁺ ions. In contrast, 3.1 eV photons excite carriers through a charge-transfer-type transition (which does not directly affect spin/orbital order), yet the resulting relaxation dynamics are still influenced by the existing spin and orbital ordered states. Our results thus show that UOS is sensitive to all three of the spin and orbital ordering transitions that have been previously measured via other techniques [8, 10] through

* Corresponding author; rpprasan@lanl.gov

[†] Corresponding author; mlee@lanl.gov

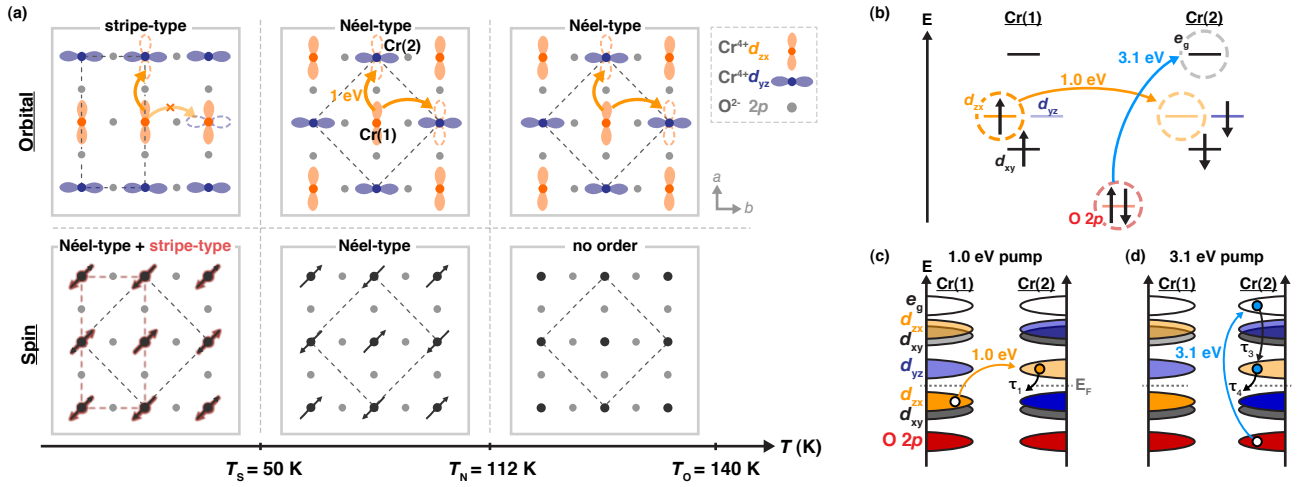


FIG. 1. (a) Schematic diagrams of the spin- and orbital-ordered ground state in α - Sr_2CrO_4 , showing different types of antiferro-type spin ordering and d_{yz}/d_{zx} orbital ordering. We note that the four-lobed shapes of the d -orbitals are projected into the ab -plane. Arrows indicate possible 1 eV transitions from occupied (filled shapes) to unoccupied (dotted shapes) orbital states in a given ordered phase; transitions from Cr(1) to Cr(2) ions are shown for simplicity, but the reverse can also occur. (b) Energy levels and orbital structures on neighboring sites with Cr(1) and Cr(2) ions for $T \leq T_N$. The d - d transitions between d_{zx} orbitals from Cr(1) to Cr(2) (or between d_{yz} orbitals from Cr(2) to Cr(1)) correspond to hopping energies of 1.0 eV. 3.1 eV excitation drives a charge-transfer-type transition from O $2p$ to Cr e_g orbitals. The relevant electronic structures are displayed along with photoexcitation at (c) 1.0 eV and (d) 3.1 eV. On-site transitions from O $2p$ to Cr e_g states are possible at both Cr(1) and Cr(2) sites.

their distinct timescales [14]. Furthermore, we provide new experimental evidence for the existence of a phase transition at T_O , with a close relation to the stripe-type spin-orbital order below T_S .

We measured the time-resolved photoinduced changes in reflectivity on an epitaxially grown, 100 nm thick c -axis oriented film of α - Sr_2CrO_4 , which is usually hard to synthesize in bulk single crystalline form [8]. Our experiments were based on a 250 kHz femtosecond (fs) regenerative amplifier producing ~ 100 fs pulses at 1.55 eV, used to probe the transient response and also to pump an optical parametric amplifier that generated the 1.0 eV pump pulses. A beta-barium borate (BBO) crystal was used to obtain the 3.1 eV pump pulses by frequency doubling the fundamental 1.55 eV pulses. We used a near normal incident geometry for both pump and probe beams, which were linearly cross-polarized along the two equivalent in-plane a -axes (since α - Sr_2CrO_4 has tetragonal symmetry). The fluence of the 1.0 eV (3.1 eV) pump pulses was set to be 600 (400) $\mu\text{J cm}^{-2}$, generating ~ 0.1 (0.05) carriers/Cr site and a lattice temperature increase < 5 K. We measured the time-resolved reflectivity data up to $t = 250$ picoseconds (ps), and verified that the measured response was linear with pump fluence up to ~ 1 mJ cm^{-2} for both 1.0 eV and 3.1 eV pumping.

To observe non-equilibrium spin and orbital ordering dynamics, we used our 1.0 eV and 3.1 eV pump pulses to drive specific transitions in the electronic structure of α - Sr_2CrO_4 . Two electrons occupy Cr $^{4+}$ t_{2g} states in α - Sr_2CrO_4 , leading to a reversed crystal splitting effect that lifts their degeneracy [9, 15]. This results in

a lower energy for the d_{xy} orbital compared to those of the d_{yz}/d_{zx} orbitals (Fig. 1(b)). Theoretical calculations of the ground state orbital structure also revealed an AF pattern in the occupancy of d_{zx} and d_{yz} orbitals on neighboring Cr $^{4+}$ ions (Cr(1) and Cr(2)) below T_O , in addition to AF spin ordering below T_N [11, 15]. These AF spin and orbital orderings produce different partial densities of states on neighboring Cr ions, resulting in an energy scale of 1.0 eV for inter-site spin hopping from Cr(1) to Cr(2) (Cr(2) to Cr(1)) sites between d_{zx} (d_{yz}) orbitals, as indicated by the orange arrows in Fig. 1 [15, 25]. Additionally, charge transfer-type transitions between neighboring oxygen $2p$ and Cr e_g orbitals occur at higher energy scales (~ 3 eV). We note that these assignments also agree with previous optical conductivity data showing clear peaks at these photon energies [12]. In our experiments, therefore, 1.0 eV photoexcitation directly perturbs spin and orbital order, while 3.1 eV photoexcitation creates carriers whose dynamics are influenced by the existing spin and orbital orders as they relax from higher energy states. We tracked the resulting dynamics with a probe photon energy of 1.55 eV, set below the charge transfer gap energy of 2.0 eV [12] to give general sensitivity to dynamics in all t_{2g} orbitals.

Figure 2 shows T -dependent transient reflectivity ($\Delta R/R$) data for both pump photon energies, revealing dynamics on both fast (sub-ps) and relatively slow timescales. After 1.0 eV photoexcitation, a step-like feature appears immediately after time $t \sim 0$ ps at high temperatures, as exemplified at 180 K, while an additional decaying component arises at low temperatures,

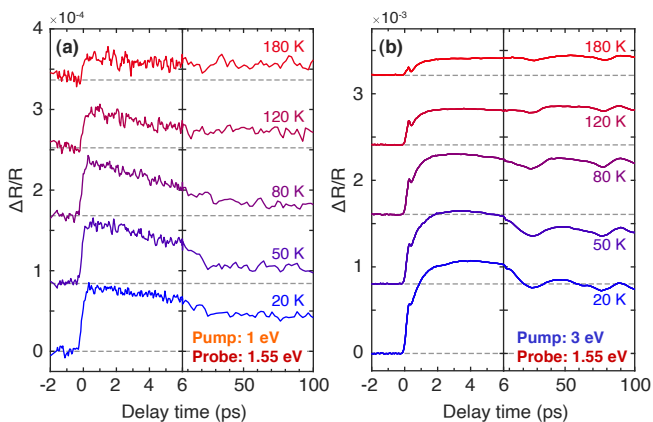


FIG. 2. Photoinduced time-resolved changes in reflectivity at 1.55 eV after (a) 1.0 eV and (b) 3.1 eV photoexcitation at various temperatures.

as seen at 20 K. In contrast, while the 1.0 eV pump data shows a monotonic decay after $t \sim 0$ ps (Fig. 2(a)), the dynamics are more complicated after 3.1 eV photoexcitation, displaying a sharp peak at $t = 0.2$ ps as well as a slowly rising component up to $t \sim 4$ ps (Fig. 2(b)). Finally, there is a slow decay at low temperatures and long time delays after both 1.0 eV and 3.1 eV photoexcitation. We note that the periodic oscillations at a frequency of 22 GHz in the transient reflectivity after 3.1 eV photoexcitation are due to optically driven acoustic phonons [25, 28]; this is well established and will not be discussed further here.

For more insight, we plotted the T -dependence of the $\Delta R/R$ signal at different time delays after 1.0 eV pumping in Fig. 3(a). $\Delta R/R$ at the peak ($t = 0.2$ ps) and $t = 4$ ps clearly deviates from the low- T linear behavior across T_N . In contrast, at longer timescales of $t = 100$ ps, we observe an increase in the $\Delta R/R$ signal below the stripe-type ordering temperature ($T_S = 50$ K). This suggests that the dynamics at short and long timescales after 1.0 eV photoexcitation are related to Néel spin order and stripe-type spin-orbital order, respectively.

To quantify the timescale for the recovery of magnetic order, we fit our data with a bi-exponential decay function, $\Delta R(t)/R = A_1 \exp(-t/\tau_1) + A_2 \exp(-t/\tau_2)$, from $t = 0.2$ ps to 200 ps, as shown in Fig. 3(b). Both the amplitude A_1 (Fig. 3(c)) and decay time τ_1 (Fig. 3(d)) of the fast component clearly show a gradual increase below T_N . Near the lowest temperatures, $\tau_1 \sim 10$ ps, revealing the timescale on which AFM order recovers after 1.0 eV excitation. Previous work on antiferromagnetic TM oxides has demonstrated that this time constant is linked to spin-lattice relaxation, i.e. photoexcited electrons rapidly transfer their energy to the lattice, which in turn equilibrates with spins on a timescale given by τ_1 [20, 21]; this is consistent with our data, and indicates that AFM order restricts carrier hopping below T_N (Fig. 1(a)). We also found that τ_2 exhibits a slower decay

time (~ 200 ps) above T_S (Fig. S3), likely due to residual lattice heating. However, below T_S , τ_2 increases up to ~ 500 ps, which may be linked to a structural change occurring concurrently with the appearance of stripe-type spin-orbital order (Fig. S6) [25].

In contrast with the transient reflectivity measured after 1.0 eV photoexcitation, which exhibited a relatively simple exponential recovery, the dynamics after 3.1 eV photoexcitation are more complex. Fig. 2(b) reveals three distinct timescales, including (1) the initial sharp peak at $t = 0.2$ ps, followed by (2) an increase up to $t \sim 4$ ps and (3) a subsequent decay on longer timescales. Fig. 4(a) shows $\Delta R/R$ as a function of T at time delays corresponding to these features. While the initial dynamics at $t = 0.2$ ps and 4 ps show only small T -dependent anomalies, $\Delta R/R$ at 100 ps changes across T_S , corresponding to the results after 1.0 eV excitation.

For a more quantitative analysis, we fit the data up to 25 ps with a model function:

$$\frac{\Delta R}{R}(t) = S(t) \times \left(1 - \exp\left(-\frac{t}{\tau_3}\right) \right) \times \left(B_1 \exp\left(-\frac{t}{\tau_4}\right) + C \exp\left(\frac{-(t-t'_0)}{\tau_p}\right)^2 \right). \quad (1)$$

While a simple two-exponential decay model was sufficient to fit the 1.0 eV data, for the 3.1 eV data we used equation (1), particularly to account for the rel-

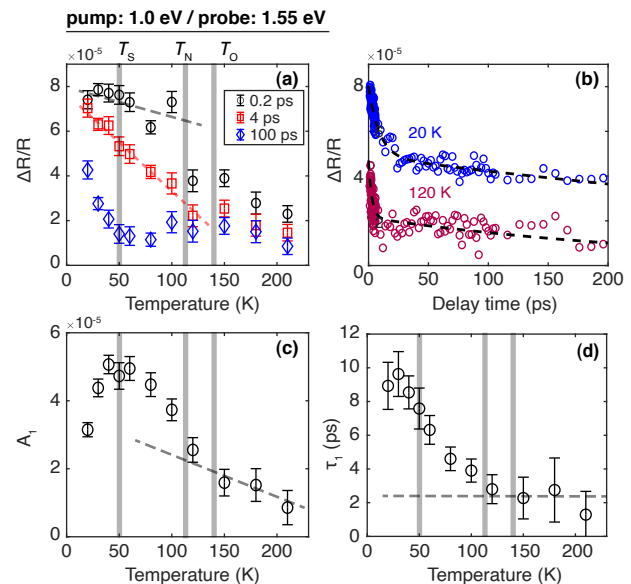


FIG. 3. Analysis of the temperature-dependent reflectivity transients after 1.0 eV photoexcitation. (a) $\Delta R/R$ at time delays of 0.2 ps (black circles), 4 ps (red squares), and 100 ps (blue diamonds). (b) Transient reflectivity data at $T = 20$ K (blue circles) and 120 K (purple circles) along with fits using bi-exponential decay functions (dashed lines). The temperature dependence of the (c) amplitude A_1 and (d) decay time τ_1 of the fast component extracted from our fits.

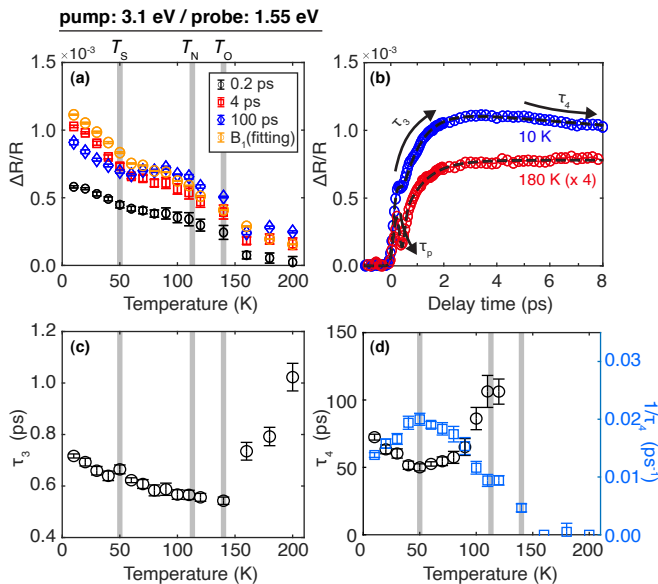


FIG. 4. Analysis of the temperature-dependent reflectivity transients after 3.1 eV photoexcitation. (a) $\Delta R/R$ at time delays of 0.2 ps (black circles), 4 ps (red squares), and 100 ps (blue diamonds). We also plot the amplitude B_1 (orange circles) obtained from our curve fits. (b) Transient reflectivity data at $T = 20$ K (blue circles) and 180 K (red circles), along with fits using the model described in the text. The data and fit curve at 180 K are scaled up by a factor of four for clear comparison. (c) The rise time (τ_3) and (d) decay time (τ_4) obtained from the ultrafast dynamics in (b), revealing a clear anomaly across $T_O = 140$ K.

atively slow rising dynamics. In this model, $S(t) = (1 + \text{erf}(t/\tau_0))/2$ is a step-function representing the convolution of the material response with the pulse duration of $\tau_0 \sim 100$ fs. We use $1 - \exp(-t/\tau_3)$ to fit the slow rising dynamics with a rise time τ_3 , and $B \exp(-t/\tau_4)$ to fit the subsequent decay with amplitude B and decay time τ_4 . The remaining part, $C_1 \exp(-(x - t'_0)/\tau_p)^2$, is used to fit the initial peak at $t'_0 \sim 0.2$ ps. The fitting results at $T = 10$ and 180 K are displayed in Fig. 4(b) with the raw data, showing that our model can accurately represent the complex dynamics triggered by 3.1 eV pumping.

The initial sharp peak may originate from several different processes, including electron-electron scattering among the photoexcited carriers [26] and two-photon absorption; additional measurements are required to conclusively determine its origin. Regardless, the initial charge transfer-type excitation between O $2p$ to Cr e_g states on neighboring ions driven by 3.1 eV photoexcitation should not directly influence magnetic or orbital order on ultrafast timescales, because neither the initial nor the final state are involved with the spin and orbital order in the Cr t_{2g} states (Fig. 1(d)).

After the initial peak, the slow rise denoted by τ_3 (Fig. 4(b)) is due to relaxation of the photoinduced carriers

from their initial e_g levels into the t_{2g} states examined by our 1.55 eV probe pulse, as indicated by the upper black arrow in Fig. 1(d). This slow rising component does not appear in the 1.0 eV data (Fig. 2(a)), since our 1.55 eV probe energy is higher than that of the 1.0 eV pump. Interestingly, τ_3 shows a clear anomaly across $T_O = 140$ K, as shown in Fig. 4(c), a transition temperature that has been observed only once via specific heat measurements [10]. This suggests that the orbital configuration changes below T_O , which can influence carrier relaxation into the conduction band minima originating from Cr t_{2g} orbitals.

The subsequent dynamics characterized by τ_4 provide further evidence of a phase transition across T_O . This time constant, which is likely due to both on-site and inter-site relaxation (discussed further below), appears below T_O and is characterized by the divergence of its decay time (Fig. 4(d)); we also plot the inverse of τ_4 to make its T -dependent anomaly at T_O clear. Additionally, τ_4 increases below T_S (Fig. 4(d)). Therefore, the relaxation dynamics occurring on a timescale of tens of ps after 3.1 eV excitation are directly linked to orbital order via the two distinct phase transitions at T_O and T_S .

For further insight into the orbital configuration, we refer to previous theoretical calculations based on a Kugel-Khomskii model (Fig. 4(a) in [8]). Considering the exchange interactions between the neighboring spins and orbitals within t_{2g} states, two different antiferro-type orbital orderings in the d_{yz} and d_{zx} states with Néel-type and stripe-type patterns can exist (Fig. 1(a)), depending on the next-nearest-neighbor exchange coupling. These calculations confirmed that the stripe-type orbital order has a lower energy, which should be accompanied by a re-configuration of the spin degrees of freedom. This agreed with RXS data showing a scattering signal consistent with stripe-type order at the lowest temperatures [8], as well as muon spin rotation data showing a second oscillatory component that may be due to coexisting stripe-type spin order [29]. These results therefore suggested that stripe-type spin-orbital order is the ground state, but AF-type orbital order can also exist in α - Sr_2CrO_4 , depending on inter-site interactions between Cr ions.

Guided by these theoretical results, our data thus suggests that the pattern of orbital order changes from stripe-type below $T_S = 50$ K to Néel-type d_{yz}/d_{zx} orbital order above T_S (Fig. 1(a)), which has been hard to observe due to the lack of clear experimental signatures, except from X-ray scattering measurements [8]. For instance, the increase in τ_4 below T_S (Fig. 4(d)) is likely due to the fact that the possible routes for inter-site hopping between the same d_{zx} (or d_{yz}) bands at nearest neighbor Cr ions are cut in half when orbital order changes from AF-type to stripe-type. More specifically, as shown in Fig. 1(a), inter-site hopping is feasible above T_S from Cr(1) to both Cr(2) nearest neighbors. However, one of these channels is blocked upon the development of stripe order, causing τ_4 to increase below T_S . In addi-

tion, we note that some fraction of the carriers photoexcited at 3.1 eV can also relax on-site (contributing to τ_4), but this process should not be directly influenced by the transition to stripe-type order at T_S . This explains the fact that we do not observe any anomaly across T_S in τ_3 (unlike in τ_4), as this component originates from on-site carrier relaxation from higher lying e_g to t_{2g} states above the Fermi level and is thus not influenced by changes from AF- to stripe-type order.

The appearance of stripe-type spin-orbital order below T_S also causes the amplitude A_1 , associated with the spin demagnetization dynamics triggered by 1.0 eV pumping, to be suppressed (Fig. 3(c)). This occurs because the probability of inter-site transitions driven by 1.0 eV photoexcitation between the same spin-polarized d_{yz} (or d_{zx}) orbitals at the nearest Cr ions in the stripe-type spin-orbital ordered phase is half of that at higher temperatures, as with τ_4 (Fig. 1(a)). However, the relevant decay time τ_1 for spin relaxation does not change abruptly across T_S , suggesting a persistent nature of the Néel-type spin order that is stable at all temperatures below T_N , though it may be accompanied by stripe-type spin order below T_S [29]. This corresponds to the previous RXS results, showing a gradual development of the Néel-type magnetic Bragg peak across T_S [8].

Finally, at higher temperatures, the T -dependent anomalies in τ_3 and τ_4 across $T_O = 140$ K most likely originate from the phase transition into the AF-type orbital ordered state. Assuming that there is no orbital order above T_O , the electronic structure for $T > T_O$ will differ from the orbital-ordered state below T_O . This is supported by the fact that the c -axis lattice constant in the CrO_6 octahedral structure decreases below T_O , as shown in Fig. S6 [9, 25]. Such distortions in the octahedral structure can change the hybridization strength between t_{2g} and e_g orbitals [30], which in turn affects the on-site relaxation of photoinduced carriers from e_g states to t_{2g} states after 3.1 eV photoexcitation (Fig. 1(d)). In other words, an increase in t_{2g} - e_g hybridization will enable photoexcited electrons in the e_g bands to scatter into the t_{2g} bands more effectively, decreasing τ_3 below T_O . Simultaneously, the photoexcited holes will hop from the O_{2p} oxygen states to either Cr(1) or Cr(2) ions, facilitating both on-site and inter-site recombination with the excess electrons in the t_{2g} bands (both processes contribute to τ_4). These considerations thus give us a general pic-

ture of carrier dynamics in α - Sr_2CrO_4 (and its sensitivity to orbital order) after 3.1 eV photoexcitation.

In conclusion, we used femtosecond optical spectroscopy to track non-equilibrium carrier dynamics in α - Sr_2CrO_4 , revealing clear temperature-dependent anomalies across the spin and orbital ordering temperatures. These experimental results are consistent with a theoretical prediction [8] of two possible orbital configurations in the d_{yz} and d_{zx} states, i.e. Néel-type order below T_O that turns into stripe-type order below T_S . Overall, our results underline the ability of ultrafast optical spectroscopy to distinguish spin and orbital orders through their timescales for coupling to the electronic structure in complex materials.

ACKNOWLEDGEMENT

This work was performed at the Center for Integrated Nanotechnologies at Los Alamos National Laboratory (LANL), a U.S. Department of Energy, Office of Basic Energy Sciences user facility, under user proposal 2018BU0083. It was primarily supported through the U.S. Department of Energy, Office of Science, Office of Basic Energy Sciences, Division of Materials Sciences and Engineering via FWP No. 2018LANLBES16 (M.-C.L. and R.P.P.). Work at MIT (C.O., J.L. Z.Z., and R.C.) was supported by the U.S. Department of Energy, Office of Science, Office of Basic Energy Sciences under Contract No. DE-SC0019126.

AUTHOR CONTRIBUTIONS

M.-C.L., R.C., and R.P.P. conceived and designed the project. α - Sr_2CrO_4 single crystalline thin films were grown and characterized by J.L., Z.Z., C.O., and R.C. M.-C.L. performed the experiments with help from N.S.S and L.T.M. The data was analyzed by M.-C.L., C.O., J.L., R.C., and R.P.P. The manuscript was written by M.-C.L. and R.P.P. with significant contributions from C.O., J.L., Z.Z., R.C., and D.A.Y.

COMPETING INTERESTS

The authors declare no competing interests.

-
- [1] Khomskii, D. I. Transition Metal Compounds. *Cambridge University Press* (2014).
 - [2] Streltsov, S. V. & Khomskii, D. I. Orbital physics in transition metal compounds: new trends. *Physics-Uspekhi* **60**, 1121 (2017).
 - [3] Imada, M., Fujimori, A. & Tokura, Y., Metal-insulator transitions. *Rev. Mod. Phys.* **70**, 1039 (1998).
 - [4] Caciuffo, R. et al. Resonant x-ray scattering study of magnetic and orbital order in KCuF_3 . *Phys. Rev. B* **65**, 174425 (2002).
 - [5] Murakami, Y. et al. Resonant X-Ray Scattering from Orbital Ordering in LaMnO_3 . *Phys. Rev. Lett.* **81**, 582 (1998).
 - [6] Rao, C. N. R. Charge, Spin, and orbital ordering in the perovskite manganates, $\text{Ln}_{1-x}\text{A}_x\text{MnO}_3$ (Ln = rare earth,

- A = Ca or Sr). *J. Phys. Chem. B* **104**, 5877 (2000).
- [7] Zegkinoglou, I. et al. Orbital ordering transition in Ca_2RuO_4 observed with resonant x-Ray diffraction. *Phys. Rev. Lett.* **95**, 136401 (2005).
- [8] Zhu, Z. H. et al. Néel and stripe ordering from spin-orbital entanglement in $\alpha\text{-Sr}_2\text{CrO}_4$. [arXiv:1906.04194](https://arxiv.org/abs/1906.04194) (2019).
- [9] Jeanneau, J. et al. Magnetism and anomalous apparently inverse Jahn-Teller effect in Sr_2CrO_4 . *Euro. Phys. Lett.* **127**, 27002 (2019).
- [10] Sakurai, H. Synthesis conditions and magnetic properties of Sr_2CrO_4 with the K_2NiF_4 -type structure. *J. Phys. Soc. Jpn.* **83**, 123701 (2014).
- [11] Pandey, B. et al. Origin of the magnetic and orbital ordering in $\alpha\text{-Sr}_2\text{CrO}_4$. *Phys. Rev. B* **103**, 045115 (2021).
- [12] Matsuno, J., Okimoto, Y., Kawasaki, M. & Tokura, Y. Variation of the electronic structure in systematically synthesized Sr_2MO_4 (M = Ti, V, Cr, Mn, and Co). *Phys. Rev. Lett.* **95**, 176404 (2005).
- [13] Zhou, H. D., Conner, B. S., Balicas, L. & Wiebe, C. R. Orbital-ordering transition in Sr_2VO_4 . *Phys. Rev. Lett.* **99**, 136403 (2007).
- [14] Giannetti, C. et al. Ultrafast optical spectroscopy of strongly correlated materials and high-temperature superconductors: a non-equilibrium approach. *Adv. in Sci.* **65**, 58 (2016).
- [15] Ishikawa, T., Toriyama, T., Konishi, T., Sakurai, H. & Ohta, Y. Reversed Crystal-Field Splitting and Spin?Orbital Ordering in $\alpha\text{-Sr}_2\text{CrO}_4$. *J. Phys. Soc. Japan* **86**, 033701 (2017).
- [16] Fausti, D. et al. Light-induced superconductivity in a stripe-ordered cuprate. *Science* **331**, 189 (2011).
- [17] Iwai, S. et al. Ultrafast optical switching to a metallic state by photoinduced Mott transition in a halogen-bridged nickel-chain compound. *Phys. Rev. Lett.* **91**, 057401 (2003).
- [18] Li, T. et al. Femtosecond switching of magnetism via strongly correlated spin?charge quantum excitations. *Nature* **496**, 69 (2013).
- [19] Prasankumar, R. P. et al. Phase inhomogeneities in the charge-orbital-ordered manganite $\text{Nd}_{0.5}\text{Sr}_{0.5}\text{MnO}_3$ revealed through polaron dynamics. *Phys. Rev. B* **76**, 020402(R) (2007).
- [20] Bowlan, P. et al. Probing ultrafast spin dynamics through a magnon resonance in the antiferromagnetic multiferroic HoMnO_3 . *Phys. Rev. B* **94**, 100404(R) (2016).
- [21] Johnson, J. A. et al., Magnetic order dynamics in optically excited multiferroic TbMnO_3 . *Phys. Rev. B* **92**, 184429 (2015).
- [22] Prasankumar, R. P. et al. Coupled charge-spin dynamics of the magnetoresistive pyrochlore $\text{Tl}_2\text{Mn}_2\text{O}_7$ probed using ultrafast midinfrared spectroscopy. *Phys. Rev. Lett.* **95**, 267404 (2005).
- [23] Lee, M.-C. et al. Strong spin-phonon coupling unveiled by coherent phonon oscillations in Ca_2RuO_4 . *Phys. Rev. B* **99**, 144306 (2019).
- [24] Coslovich, G. et al. Ultrafast dynamics of vibrational symmetry breaking in a charge-ordered nickelate. *Sci. Adv.* **3**, e1600735 (2017).
- [25] See the supplementary material for additional experimental details.
- [26] Kurz, H., Kuett, W., Seibert, K. & Strahlen, M. Hot carrier relaxation in highly excited III?V compounds. *Solid State Electron.* **31**, 447 (1988).
- [27] Cho, G. C., Kütt, W. & Kurz, H. Subpicosecond time-resolved coherent-phonon oscillations in GaAs. *Phys. Rev. Lett.* **65**, 764 (1990).
- [28] Thomsen, C., Grahn, H. T., Maris, H. J. & Tauc, J. Surface generation and detection of phonons by picosecond light pulses. *Phys. Rev. B* **34**, 4129 (1986).
- [29] Sugiyama, J. et al., Microscopic magnetic nature of K_2NiF_4 -type 3d transition metal oxides. *J. Phys. Conf. Ser.* **551**, 012011 (2014).
- [30] Landron, S. and Lepetit, M.-B. Importance of $t_{2g}\text{-}e_g$ hybridization in transition metal oxides. *Phys. Rev. B* **77**, 125106 (2008).